

Network theory approach for data evaluation in the dynamic force spectroscopy of biomolecular interactions

JELENA ŽIVKOVIĆ¹ MARIJA MITROVIĆ³ LUUK JANSSEN² HANS A. HEUS² BOSILJKA TADIĆ³ SYLVIA SPELLER¹

¹ *Scanning Probe Microscopy Group, Institute for Molecules and Materials, Radboud University, Nijmegen, Netherlands* ² *Department of Biophysical Chemistry, Institute for Molecules and Materials, Radboud University, Nijmegen, Netherlands* ³ *Department of theoretical physics, Jožef Stefan Institute, Ljubljana, Slovenia*

PACS 89.75.Hc – Networks and genealogical trees

PACS 82.37.Rs – Single molecule manipulation of proteins and other biological molecules

PACS 02.70.Hm – Spectral methods

Abstract. - Investigations of molecular bonds between single molecules and molecular complexes by the dynamic force spectroscopy are subject to large fluctuations at nanoscale and possible other aspecific binding, which mask the experimental output. Big efforts are devoted to develop methods for effective selection of the relevant experimental data, before taking the quantitative analysis of bond parameters. Here we present a methodology which is based on the application of graph theory. The force–distance curves corresponding to repeated pulling events are mapped onto their correlation network (mathematical graph). On these graphs the groups of similar curves appear as topological modules, which are identified using the spectral analysis of graphs. We demonstrate the approach by analyzing a large ensemble of the force–distance curves measured on: ssDNA–ssDNA, peptide–RNA (system from HIV1), and peptide–Au surface. Within our data sets the methodology systematically separates subgroups of curves which are related to different intermolecular interactions and to spatial arrangements in which the molecules are brought together and/or pulling speeds. This demonstrates the sensitivity of the method to the spatial degrees of freedom, suggesting potential applications in the case of large molecular complexes and situations with multiple binding sites.

Introduction. – It has been recognized recently [1] that the signals generated at a single molecule (or another nano-size object) differ from signals obtained in large-scale systems consisting of ensemble of molecules. In particular, enhanced fluctuations, randomness and irreproducibility of the signals are observed in single-molecule measurements. A representative example is the mechanical signal generated in the dynamic force spectroscopy (DFS) of molecular bonds [2, 3]. The force spectroscopy of single molecules and molecular complexes has become a leading methodology for measuring biomolecular unbinding forces, which form the bases of biologically relevant molecular processes [4]. For instance, some recently studied examples include measurements of fundamental biomolecular forces in DNA unzipping [5], ALCAM-ALCAM [6], peptide- antibody [7], RNA- protein [8] interactions, etc.

In a typical pulling experiment in DFS based on the Atomic Force Microscopy, the ligand and receptor molecule are attached via polymer linkers on the AFM

tip and the solid support (e.g glass, mica, gold- surface). The molecules are brought close to each other for certain contact time allowing them to form a bond and then pulled away until the bond breaks. The process is repeated many times. In each pulling event, changes in the deflection of the AFM cantilever as a function of distance are measured. Knowing the spring constant of the cantilever, this data can be calculated into distance dependent forces, resulting in so called force-distance curves. From these curves different parameters can be obtained, such as force needed to break a certain bond and the force loading rate. Further quantitative analysis of these data sets requires an elaborated theoretical framework [2] in order to extract the parameters of binding potential, the bond strength and the survival time. The applied force reduces the barrier between the bound and dissociated states of the binding molecules, allowing to estimate the force at which the barrier disappears and to measure the dissociation rate $\lambda(F)$. Then the *natural* dissociation rate at vanishing force is ex-

tracted using an appropriate theoretical framework. Since the pioneering work [2], assuming the exponential dependence of the dissociation rate on the applied force, the theory of the dynamic force spectroscopy evolved in two major directions: (i) incorporating a phenomenological distribution of the bond parameters [9], and (ii) assuming a specific type of the binding potential, from which the dissociation rate $\lambda(F)$ is computed exactly [10, 11].

The pulling–disruption process of the molecular bonds, for instance in constant-velocity experiments used in this work, is both nonlinear and stochastic. Nonlinearity, which is manifested in force-dependent loading rate $\dot{F}(F)$, can be related to the internal degrees of freedom of the (large) molecules and the spacers. Fluctuations in the disruption force and loading rate originate from the diffusion of binding molecules in solvent, whose effects depend on the binding potential and pulling speed. Thus the bond parameters can be determined in terms of probability, using the appropriate theoretical concept. In addition to the molecular bond of interest (specific binding), other non-specific processes may occur at the same contact time and range of forces: mis-binding or binding at different site, or unspecific interaction of the molecule with linkers and surface. It is, therefore, of great importance to be able to select the force–distance curves which are related to true binding *prior* to the quantitative analysis of the bond parameters. It is a general believe (see also discussion in [12]) that, apart from the fluctuations, *the force–distance curves originating from the same binding process share strong similarity*. Given a large amount of data in a particular experiment, this is a technically demanding task, which requires automated computational approach. Recently two methods were proposed based on pattern-recognition [13] and master-curve fitting [12].

In this work we present a new approach for systematic selection of groups of mutually similar force–distance curves and demonstrate it on sets of data from peptide–RNA complex from HIV1. Our methodology is based on the theory of complex networks and their spectral analysis [14–16]. Mapping multichannel datasets onto a network representation has proved as a useful tool [17] in the analysis of many complex dynamical systems, for example stock-market time series [18], gene-expression signals [19, 20], neural activity signals [21–23], climate phase fluctuations [24], and information traffic time series [25]. Compared to these examples, where the time-series are measured at each unit of an extended interacting system, our approach here is to map the force–distance signal measured in repeated experiments on the same molecular complex with many degrees of freedom. To demonstrate our approach, we analyze a large dataset of force–distance curves measured under different conditions in RNA–peptide complex (HIV1-Rev peptide binding at the high affinity site in the stem-loop of the RRE on viral RNA) [26] and, for comparison, a set of curves for ssDNA–ssDNA binding and two control sets. The filtered correlation matrix mapped onto a binary graph exhibits mod-

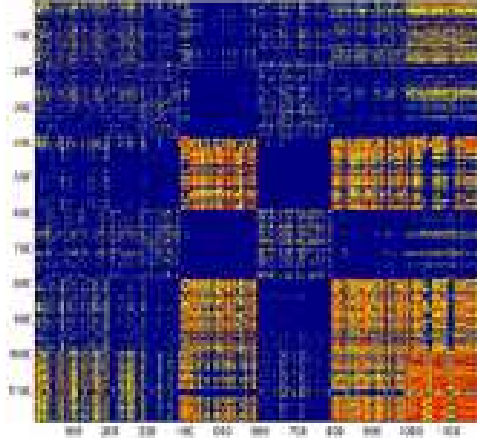


Fig. 1: Correlation matrix of different types of force curves, described in the text. Color intensity from blue (low) to red (high) indicates the strength of correlation C_{ij} between pairs of curves. Shown are correlations after matrix filtering and above a threshold $C_{ij} > 0.5$.

ular structure, with the subgraphs of nodes (curve index) grouped according to their similarity over the entire data sets. We then look for the force-curves in each of the subgraphs and find the underlying reasons for their clustering.

Description of the Experimental Data. – We created the correlation matrix from all pairs of $N = 1188$ force curves, that were pre-processed in the following way: contact part was removed, curves were corrected to the baseline, and only the part where interactions are expected was kept (first 200nm). Curves for the correlation matrix were selected from four different experiments with two different experimental setups. The experiential setups differ in the number of flexible linkers used to couple molecules to the surface and the cantilever: either both molecules were coupled to the cantilever/surface via PEG spacers or one was coupled to the gold surface directly and the other to the cantilever via PEG spacer. In the correlation matrix (see Fig. 1 and text below), from left-to-right, the first block (I) consists of 200 curves taken from measurements on RNA–Rev peptide interaction (two linkers, velocity 581nm/s); second block (II) consists of 188 curves taken from RNA–Rev peptide interaction in the presence of neomycin (two linkers, velocity 581nm/s); third block (III) contains 200 curves measured on RNA–Rev peptide interaction (one linker, velocity 2540nm/s); fourth block (IV) contains 200 curves measured on ssDNA–ssDNA interaction (two linkers, velocity 218nm/s); fifth block (V) has 200 curves of RNA–Rev peptide interaction (one linker, velocity 1160nm/s), and the last block (VI) consists of 200 curves of Rev peptide–Au interaction (one linker, velocity 1160nm/s).

Correlation Matrix and its Spectral Analysis.

– In our dataset consisting of $N = 1188$ force–distance curves, $\{f_i(x)\}$, $i = 1, 2, 3, \dots, N$, each curve is identified by a uniquely defined index i , thus representing a separate pulling event. The elements of the correlation matrix C_{ij} are calculated as the Pearson’s correlation coefficient between each pair (i, j) of curves as follows:

$$C_{ij} = \frac{\sum_k [f_i(x) - \langle f_i \rangle][f_j(x) - \langle f_j \rangle]}{\sigma_i \sigma_j}. \quad (1)$$

where the distance x is given by a discrete set of measured values, and σ_i , σ_j stand for the standard deviation of the force signal $f_i(x)$ and $f_j(x)$. In Fig. 1 we show a 3D color plot of the correlation matrix of all force curves, after filtering out spurious correlations. For the filtering, we used the affinity transformation method [22, 25], where the element is enhanced as $C_{ij} \rightarrow M_{ij}C_{ij}$ if the rows i and j correlate with the rest of the matrix in a similar way, yielding $M_{ij} > 1$, and diminished otherwise. The meta-correlation factor M_{ij} is computed as a Pearson’s coefficient of the rearranged elements $\{C_{ij}, C_{i1}, \dots, C_{i-1j}, C_{i+1j}, \dots, C_{iN}\}$ and $\{C_{ji}, C_{j1}, \dots, C_{j-1i}, C_{j+1i}, \dots, C_{jN}\}$ without diagonal.

For further discussion we notice that the matrix can be represented by a network (mathematical graph), where each matrix index $i = 1, 2, \dots, N$ defines network node and the matrix element C_{ij} —a link between nodes i and j . In our case the links are symmetrical $C_{ij} = C_{ji}$ by definition (1). Notice that the matrix and network representations are formally equivalent. The network picture is suitable for visualization and topological interpretation. In particular, the matrix in Fig. 1 makes a sparse network containing topological *modules*, i.e., groups of nodes with strong connections inside the group and sparse connections between them. As the Fig. 1 shows, correlations between different sets of data (blocks I through VI) shown as off-diagonal block-matrices can be as strong as correlations inside the same data set (diagonal blocks). This suggests that the network modules may contain curves from different data blocks! In the following we apply the eigenvalue spectral methods to identify these topological modules.

Here we perform spectral analysis of the normalized Laplacian operator \mathbf{L} related to the filtered correlation \mathbf{C} in Fig. 1, or more precisely, its binary form with the elements: $A_{ij} = 1$ whenever $C_{ij} > C_0$, or $A_{ij} = 0$ otherwise. The matrix elements of the Laplacian are given by [16, 27]

$$L_{ij} = \delta_{ij} - \frac{A_{ij}}{\sqrt{q_i q_j}}, \quad (2)$$

where q_i , q_j are the number of links at nodes i and j , respectively. Although the same conclusions can be reached using the adjacency matrix A_{ij} directly, the analysis of the Laplacian (2) is more convenient since its eigenvalue spectrum is limited in the range $\lambda_i \in [0, 2]$. Moreover, its *eigenvectors belonging to few lowest nonzero eigenvalues tend to localize along the network modules* [15, 16]. This

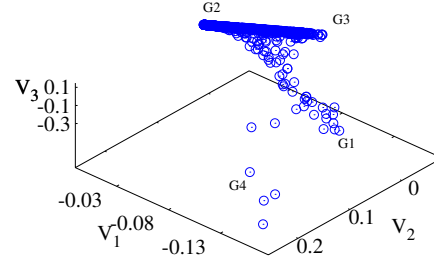


Fig. 2: Scatterplot of the eigenvectors V_1, V_2, V_3 of three lowest eigenvalues of the Laplacian operator (2) related to the full correlation matrix in Fig. 1. Four branches are visible in this projection, marked as G_1, G_2, G_3, G_4 .

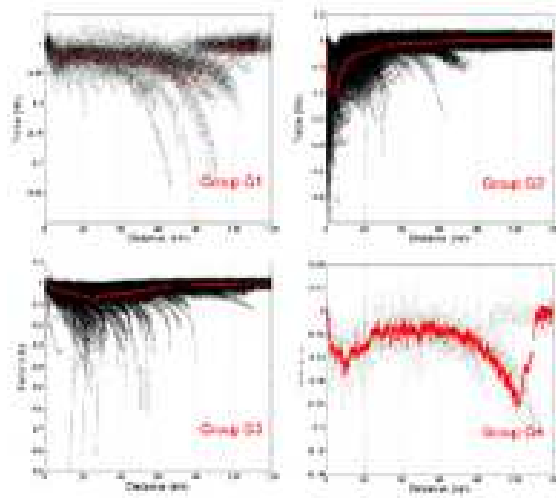


Fig. 3: Overlap plot of all curves belonging to the groups G_1, G_2, G_3, G_4 identified from the scatterplot in Fig. 2.

is a direct consequence of the orthogonality to the eigenvector belonging to zero eigenvalue of the Laplacian (or the largest eigenvalue of the adjacency matrix) which has all positive components (Perron-Frobenius theorem [28]). Precisely, the localization means that, among N components of the eigenvector, the nonzero (positive/negative) components have indexes which coincide with nodes in a network module (detailed analysis of spectra in modular networks is given in [16]). We use this property of the eigenvectors to identify nodes in different modules.

Identification of modules: Force-curves grouping. – When a modular structure occurs, the localization of eigenvectors belonging to smallest non-zero eigenvalues is manifested in a *branched* pattern of the scatterplot in the space of these eigenvectors [16]. In Fig. 2 we show the scatterplot of the eigenvectors (V_1, V_2, V_3) belonging for three smallest non-zero eigenvalues of the Laplacian (2), related to the correlation matrix in Fig. 1. In the scatterplot, each point carries one index, thus

Table 1: (upper part) Representative curves appearing at tips of four branches G_1, G_2, G_3, G_4 in the scatterplot in Fig. 2 and their distribution over original blocks of data I through VI. (Middle and bottom) Further splitting of groups G_2 and G_3 .

block	I	II	III	IV	V	VI
G1	5	9	0	16	0	0
G2	51	28	177	0	181	148
G3	60	68	0	135	1	7
G4	4	0	1	0	0	0
G2-g1	5	1	3	0	35	22
G2-g2	0	0	45	0	7	0
G2-g3	20	10	5	0	3	21
G3-g1	5	6	0	24	1	0
G3-g2	24	9	0	24	0	5
G3-g3	18	15	0	28	0	1



Fig. 4: Example of the correlation network constructed from the force curves in group G_2 from Fig. 2, exhibiting modular structure. Shown are only links above the threshold $C_0 = 0.91$.

indicating one network node, that is a force curve index in our original dataset. The plot in Fig. 2 shows four branches, marked by G_1, G_2, G_3, G_4 , thus four groups of curves can be identified. The most representative curves in each group are those at the tips of branches with most distinct curves sitting at the opposite ends of the branches G_2 and G_3 , whereas, the differences gradually diminishes closer to the center of the plot. By matching the indexes with curves in the original dataset, we identify representative curves at the tips of four branches (Table 1.). Overlay of all curves in the $G_1 \dots G_4$ groups is shown in Fig. 3.

Each of the groups contains number of curves from one or several blocks of the original datasets. Recalling the nature of the data in different blocks, we see that the module G_2 contains curves obtained predominantly on experimental setup with one PEG spacer (blocks III, V, and VI) and a fraction of data with two spacers (from blocks I and II), while excluding altogether the DNA-DNA interactions

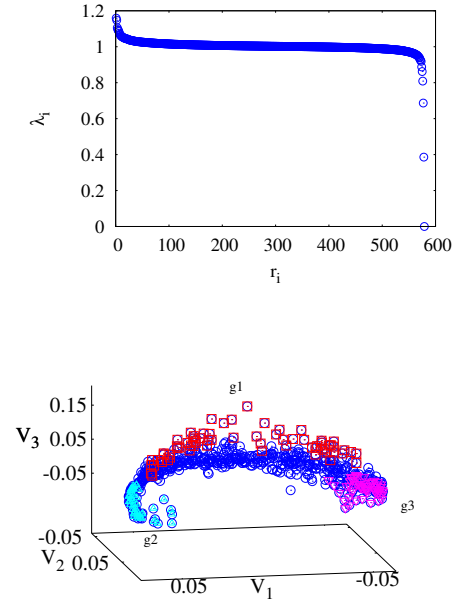


Fig. 5: For the branch G_2 of Fig. 2: (top) the eigenvalue spectrum and (bottom) the scatterplot of three eigenvectors belonging to lowest nonzero eigenvalues. Three subgroups are identified marked by g_1, g_2, g_3 , see text for details.

(block IV). On the other hand, the module G_3 contains data from DNA-DNA interactions and a number of curves from Rev-RNA and blocked Rev-RNA with neomycin, all data obtained using two spacers. G_1 has similar composition although it appears as a separate module, similar as the small group G_4 (see visual differences in Fig. 3).

We further analyze the group of curves in G_2 applying the same approach on the now reduced correlation matrix. The complete group consists of $N_2 = 597$ curves. The correlation network of these curves, shown in Fig. 4, exhibits modular structure, suggesting that smaller subgroups of the group G_2 can be identified. The eigenvalues of the Laplacian related to this correlation matrix are shown in the ranking order in Fig. 5, top panel. Compatible with the network modularity in Fig. 4 is the appearance of three eigenvalues in the gap between $\lambda = 0$ and the main part of the spectrum. The corresponding scatterplot in the space of three eigenvectors belonging to these eigenvalues is also shown in Fig. 5, bottom panel. In this case similarity between points, forming a half-helmet in (V_1, V_2, V_3) space, is stronger compared to Fig. 2, however, groups can be identified by the end points of the half-ring in the horizontal plane and points with largest vertical distance, marked as g_1, g_2, g_3 and different symbols (colors) in Fig. 5.

The identity of these curves with respect to the original datasets is also indicated in Table 1, middle part. As mentioned above, curves in large group G_2 are on Rev peptide binding, whereas, their subgroups appear to be from different pulling velocities: $G_2 - g_1$ consists mostly

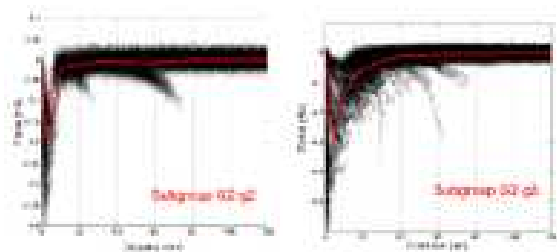


Fig. 6: Overlay of the selected force curves of low- and high-velocity associated to ends of the scatterplot ring in Fig. 5.

of curves in blocks V and VI, measurements at velocity of 1160 nm/sec, while the groups $G_2 - g_2$ and $G_2 - g_3$ at two ends of the semi-ring contains curves measured at highest (2540 nm/sec) and lowest (581 nm/sec) velocity, respectively. In the experiment, measurements at different velocities and correct assignments of the curves are important for the extrapolation of bonding parameters to zero force values. Pulling velocity affects both force loading rate $\dot{F}(F)$ as well as the average disruption force $\langle F \rangle$. Within our methods selected groups of high- and low-velocity curves, $G_2 - g_2$ and $G_2 - g_3$, respectively, are shown in Fig. 6. Similar analysis of the data contained in the group G_3 (not shown) leads to the curves identified in the lower part of the Table 1. Here data contain three different interactions (DNA-DNA, Rev-RNA, and Rev-RNA-with-neomycin), all measured in the setup with two spacers and low velocity. We find much larger mixing between the groups, indicating either increased number of specific binding or a dominant role of spacers.

Finally, in Fig. 7 we show histograms of the rupture forces made upon curves in groups G_2 and G_3 selected by our methodology. Detailed analysis of Rev-RNA bonding parameters is given in [26].

Conclusions. – We have shown that stochastic signals of different molecular systems (peptide-RNA, DNA-DNA) measured in the dynamic force spectroscopy experiments can be effectively selected according to their similarities. Our methodology uses the signal’s relevant correlation matrix mapped onto a mathematical graph. Then using the spectral analysis of these graphs the groups of similar curves are detected, which appear as topological modules on them. Although the method is essentially statistical, we have shown that strong regularities in groupings of the force curves occur (and can be effectively used for the signal evaluation), based on the pulling speeds and experimental setup and even type of the interaction measured. Note that for the demonstration purposes in this work we used raw data with minimal pre-processing. Further pre-processing, e.g., with curve-fitting [12], could be incorporated and increase selectivity in our method. Improved efficiency in the evaluation of force curves by this approach is also expected in the case of larger molecules or molecular complexes and the situations where distinction between many binding sites is applicable.

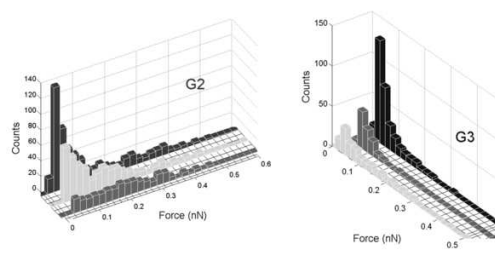


Fig. 7: Histograms of rupture forces from selected curves in blocks VI, V, III from group G_2 (left) and from blocks I, II, IV from group G_3 (right). (Cf. Table 1. and data description.)

* * *

Work supported by the FP6 project Functional and Structural Genomics on Viral RNA: FSG-V-RNA, the FP7 project CYBEREMOTIONS, and the Nanotechnology programme of the Ministry of Economic Affairs, NanoNed (Netherlands) and the national program P1-0044 (Slovenia). J.Ž. also thanks for the hospitality during her stay at the J. Stefan Institute, Ljubljana.

REFERENCES

- [1] E. Barkai, F. Brown, M. Orrit, and H. Yang, *Theory and evaluation of single-molecule signals*. World Scientific, Singapore, 2008.
- [2] E. Evans and K. Ritchie, “Dynamic strength of molecular adhesion bonds,” *Biophysical Journal*, vol. 72, pp. 1541–1555, 1997.
- [3] T. Strunz, K. Oroszlan, R. Schäfer, and H. Güntherodt, “Dynamic force spectroscopy of single dna molecule,” *PNAS*, vol. 96, no. 41, pp. 11277–11282, 1999.
- [4] J. Zlatanova, S. Lindsay, and S. Leuba *Prog. Biophys. Mol. Biol.*, vol. 74, p. 37, 2000.
- [5] S. Koch and M. Wang, “Dynamic force spectroscopy of protein-dna interactions by unzipping dna,” *Phys. Rev. Lett.*, vol. 91, p. 028103, Jul 2003.
- [6] J. te Riet, A. Zimmerman, A. Cambi, B. Joosten, S. Speller, R. Torensma, F. van Leeuwen, C. Figdor, and F. de Lange, “Distinct kinetic and mechanical properties govern alcam-mediated interactions as shown by single-molecule force spectroscopy,” *Journal of Cell Science*, vol. 120, pp. 3965–3976, 2007.
- [7] T. Sulchek, R. Friddle, K. Langry, E. Lau, H. Albrecht, V. Ratto, S. DeNardo, M. Colvin, and A. Noy, “Dynamic force spectroscopy of parallel individual mucin1-antibody bonds,” *PNAS*, vol. 102, pp. 16638–16643, 2005.
- [8] A. Fuhrmann, J. Schoening, D. Anselmetti, D. Staiger, and R. Ros, “Quantitative analysis of single-molecule rna-protein interaction,” *Biophysical Journal*, **96**, 5030, 2009.
- [9] M. Raible, M. Evstignev, F. Bartels, R. Eckel, M. Nguyen-Duong, R. Merkel, R. Ros, D. Anselmetti, and P. Reimann, “Theoretical analysis of single-molecule force spectroscopy experiments: Heterogeneity of chemical bonds,” *Biophysical Journal*, vol. 90, p. 3851, 2006.

- [10] O. Dudko, G. Hummer, and A. Szabo, “Intrinsic rates and activation free energies from single-molecule pulling experiments,” *Phys. Rev. Lett.*, vol. 96, p. 108101, 2006.
- [11] O. Dudko, G. Hummer, and A. Szabo, “Theory, analysis, and interpretation of single-molecule force spectroscopy experiments,” *PNAS*, vol. 105, pp. 15755–15760, 2008.
- [12] A. Fuhrmann, D. Anselmetti, and R. Ros, “Refined procedure of evaluating experimental single-molecule force spectroscopy data,” *Phys. Rev. E*, **77**, 031912, 2006.
- [13] A. Marsico, D. Labudde, T. Sapra, D. Muller, and M. Schroeder, “A novel pattern recognition algorithm to classify membrane protein unfolding pathways with high-throughput single-molecule force spectroscopy,” *Bioinformatics*, vol. 23, no. 2, pp. e231–e236, 2005.
- [14] S. Boccaletti, V. Latora, Y. Moreno, M. Chavez, and D. U. Hwang, “Complex networks: Structure and dynamics,” *Physics Reports*, vol. 424, p. 175, 2006.
- [15] L. Donetti and M. A. Muñoz, “Detecting network communities: a new systematic and efficient algorithm,” *Journal of Statistical Mechanics: Theory & Experiment*, **10**, 2004.
- [16] M. Mitrović and B. Tadić, “Spectral and dynamical properties in classes of sparse networks with mesoscopic inhomogeneities,” *Physical Review E*, vol. 80, no. 1, 2009.
- [17] I. Baruchi, D. Grossman, V. Volman, M. Shein, J. Hunter, V. Towle, and E. Ben-Jacob, “Functional holography analysis: Simplifying the complexity of dynamical networks,” *Chaos*, vol. 16, p. 015112, 2006.
- [18] R. N. Mantegna, “Hierarchical structure in financial markets,” *European Physical Journal B*, vol. 11, p. 193, 1999.
- [19] J. Živković, B. Tadić, N. Wick, and S. Thurner, “Statistical indicators of collective behavior and functional clusters in gene networks of yeast,” *European Physical Journal B*, vol. 50, pp. 255–258, 2006.
- [20] J. Živković, M. Mitrović, and B. Tadić, “Correlation Patterns in Gene Expression along the Cell Cycle of Yeast,” *Springer Series: Studies in Computational Intelligence*, vol. 207, pp. 23–34, 2009.
- [21] L. Zemanova, C. Zhou, and J. Kurths, “Structural and functional clusters of complex brain networks,” *Physica D: Nonlinear Phenomena*, vol. 224, pp. 202–212, 2006.
- [22] I. Baruchi and E. Ben-Jacob, “Functional holography of recorded neuronal networks activity,” *Neuroinformatics*, vol. 2, no. 3, pp. 333–351, 2004.
- [23] R. Graben, C. Zhou, M. Thiel, and J. Kurths, *Lectures in Supercomputational Neuroscience: Dynamics in Complex Brain Networks (Understanding Complex Systems)*. Springer-Verlag, Berlin Heidelberg, 2008.
- [24] K. Yamasaki, A. Gozolchiani, and S. Havlin, “Climate networks based on phase synchronization analysis track el-nino,” *Prog. Theor. Phys. Suppl.*, vol. 179, p. 178, 2009.
- [25] B. Tadić and M. Mitrović, “Jamming and correlation patterns in traffic of information on sparse modular networks,” *European Physical Journal B*, 2009.
- [26] J. Živković, L. Jansen, F. Alvarado, H. Heus, and S. Speller, “Force spectroscopy on RRE-Rev complex from HIV1,” *in preparation*, 2009.
- [27] A. N. Samukhin, S. N. Dorogovtsev, and J. F. F. Mendes, “Laplacian spectra of, and random walks on, complex networks: Are scale-free architectures really important?,” *Physical Review E*, vol. 77, no. 3, pp. 036115–+, 2008.
- [28] C. Godsil and G. Royle, *Algebraic Graph Theory*. Springer-Verlag, Berlin Heidelberg, 2001.